Available online at www.sciencedirect.com
ScienceDirect
Physica B 401–402 (2007) 511–518
PHYSICA B
www.elsevier.com/locate/physb

Defect studies for the development of nano-scale silicon diffusion simulators

Masashi Uematsu*, Yasuo Shimizu, K.M. Itoh

Faculty of Science and Technology, Keio University, Yokohama 223-8522, Japan

Abstract

Fabrication of the next generation silicon devices requires fundamental understanding of defect interactions that are characteristic of nano-scale device processing. Because a variety of intrinsic and extrinsic defects generated at surfaces and interfaces can easily diffuse and reach the active regions in the nano-scale devices, it becomes crucial to understand the transient and non-equilibrium behaviors of defect interactions related to nano-scale fabrications. In order to identify what types of kinetics and reactions are relevant to nano-processing, diffusion in silicon and silicon oxide is studied using isotopically controlled silicon heterostructures. Our experiments probing the effect of interfaces on impurity and silicon self-diffusion in silicon dioxide, silicon self-diffusion in silicon, and implanted-impurity and silicon interactions are reviewed. Then quantitative models based on such experimental studies are presented and how they will be utilized in the construction of diffusion simulators is discussed.

Keywords: Silicon; Silicon oxide; Interface; Defects; Diffusion; Nano-process; Simulation

1. Introduction

Nanoscience and nanotechnology offer challenging issues to fundamental research and in addition new opportunities for innovative industrial applications. When silicon devices are developed on a nano-scale, the atomic and molecular behavior becomes different from the one observed on the micro-scale. Because a variety of intrinsic and extrinsic defects generated at surfaces and interfaces can easily diffuse to reach the active regions in nano-scale devices, it becomes crucial to understand transient and non-equilibrium behaviors of relevant defects, which are greatly affected by the surfaces and interfaces. Besides, simulation has become an indispensable tool for the development and optimization of silicon processes, and the development of nano-process simulators requires fundamental understanding of defect interactions that are characteristic of the nano-scale device processing. Therefore, nano-process design requires solid understanding of the transient and non-equilibrium nature of defect interactions related to the nano-CMOS (complementary metal oxide semiconductor) device fabrications.

Among several characteristic features of nano-scale processing, the following points are especially highlighted with the scaling down of CMOS devices:

1. Diffusion and reaction in the bulk are more likely to be affected by defects that are generated at interfaces to induce transient and non-equilibrium phenomena because the bulk materials of interest are closer to interfaces, such as silicon/dioxide interfaces (Si/SiO_2).
2. The temperatures used in nano-processes become lower in order to reduce the impurity diffusion during annealing. Low-temperature processes are likely to prolong the duration of transient and non-equilibrium behaviors of defects. In addition, the crossover from one diffusion mechanism at high temperatures to the other at low temperatures becomes crucial when two diffusion mechanisms are involved.
3. The impurity concentration in the source and drain regions of CMOS devices should be increased to maintain a low device resistance. High-concentration impurity diffusion often generates non-equilibrium

*Corresponding author. Tel.: +81 45 566 1594;, fax: +81 45 566 1587.
E-mail address: uematsu@a3.keio.jp (M. Uematsu).

0921-4526/$ - see front matter © 2007 Elsevier B.V. All rights reserved.
doi:10.1016/j.physb.2007.09.011

point defects. In addition, higher dose ion implantation will induce more severe supersaturation of silicon self-interstitials.

These characteristic features include the transient and non-equilibrium nature of defect interactions in nano-processing. In order to identify what types of kinetics and reactions are relevant to the nano-processing, it is indispensable to precisely investigate not only the behavior of impurity atoms but also that of silicon atoms in silicon, that is, silicon self-diffusion. We have studied self-diffusion in silicon oxide [1–3] and silicon [4] using silicon isotope heterostructures and superlattices to understand the fundamental behaviors of defects. We will review our experiments probing the emission of defects from the Si/SiO_2 interface into the oxide in Section 2. Next, silicon self-diffusion experiments in silicon at low temperatures are presented in Section 3. Then, simultaneous observation of the behavior of impurities and silicon atoms in silicon isotope superlattices is presented in Section 4. In these sections, we will present quantitative models based on such experimental studies and discuss how they will be utilized in the construction of the useful diffusion process modeling.

2. Effect of the Si/SiO_2 interface on diffusion in SiO_2

As the thickness of SiO_2 layers for CMOS devices decreases, diffusion in SiO_2 becomes one of the fundamental issues. Concerning impurity diffusion, boron (B) penetration from the gate electrode through the thin SiO_2 layer into the Si substrate is a serious problem [5], and a precise simulation of B diffusion in SiO_2 is essential. The diffusion in SiO_2 is also an important issue in high-k gate dielectrics because an interfacial SiO_2 layer forms between high-k gate films and Si substrates during post-annealing [6]. Therefore, we have investigated not only B diffusion but also Si self-diffusion in SiO_2 in order to elucidate the defects that mainly contribute to B diffusion [1–3]. An isotopically enriched ^{28}Si single-crystal epi-layer was thermally oxidized in dry O_2 at 1100 °C to form $^{28}SiO_2$ of thicknesses of 200, 300, and 650 nm. The samples were implanted with ^{30}Si at 50 keV to a dose of $2\times10^{15}\,cm^{-2}$ and capped with a 30-nm-thick silicon nitride layer. The sample structure is shown in Fig. 1. In addition, uncapped samples were also used. Samples were pre-annealed at 1000 °C for 30 min to eliminate implantation damage and diffusion-annealed at temperatures between 1150 and 1250 °C. Annealing was conducted in flowing argon with 1% oxygen, which is just enough to prevent SiO_2 decomposition. The depth profiles of ^{30}Si were measured by secondary ion mass spectrometry (SIMS).

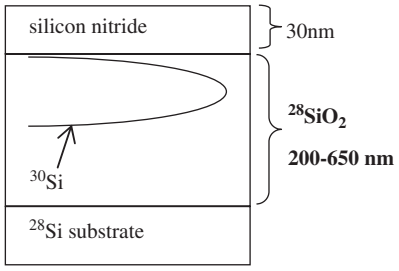

Fig. 1. The sample structure.

Fig. 2 shows the experimental ^{30}Si depth profiles of samples before and after diffusion annealing for 168 h at 1200 °C. The as-implanted ^{30}Si profile before pre-annealing is shown as the initial profile because the profile after the pre-annealing showed no observable diffusion within the accuracy of our SIMS measurements. The samples demonstrate a strong dependence on the thickness of the $^{28}SiO_2$ layer; the thinner the $^{28}SiO_2$ layer is, the broader the

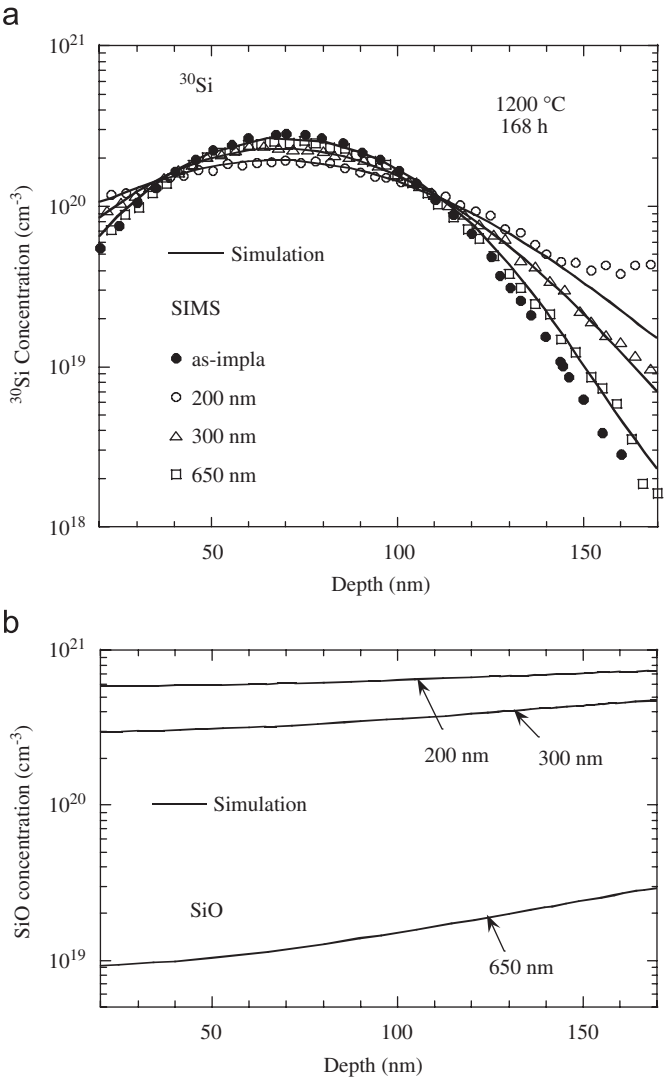

Fig. 2. (a) Simulated and experimental ^{30}Si depth profiles and (b) simulated SiO profiles in the SiO_2 samples with various thicknesses. Samples were annealed at 1200 °C for 168 h. The as-implanted ^{30}Si profile is shown as the initial profile. In SIMS data, the increase of ^{30}Si concentration deep in the bulk (>150 nm) in the 200-nm-thick sample is ^{30}Si that diffused from ^{nat}Si substrates (800 nm below the ^{28}Si epi-layer) during the thermal oxidation to prepare the sample. (^{nat}Si refers to Si with the natural isotopic abundance.)

diffusion profile becomes. In other words, the Si self-diffusivity increases with decreasing the distance between the diffusing ^{30}Si species and $^{28}Si/^{28}SiO_2$ interface. In contrast, the Si self-diffusivity of uncapped samples showed no significant dependence on the $^{28}SiO_2$ thickness, and the diffusivity values agreed with the thermal equilibrium values obtained from damage-free CVD (chemical vapor deposition) SiO_2 [7]. This tendency was observed consistently for other temperatures and annealing times employed in this study. As a possible origin of the distance dependence of Si self-diffusion, we examined the effect of implantation damage; however, we found that it is of no concern because the self-diffusivity of implanted Si in thick SiO_2 agrees with the thermal Si self-diffusivity [7] and remains unchanged for the ^{30}Si doses between 1×10^{14} and $2\times10^{15}\,cm^{-2}$. In addition, we have performed an experiment using CVD isotope heterostructures with a constant total oxide thickness and found that the Si self-diffusivity increases with decreasing the distance from the interface in the same way as that described above [8].

These results lead us to conclude that Si species generated at the Si/SiO_2 interface and diffusing into SiO_2 enhance Si self-diffusion in SiO_2. As the dominant Si species, SiO generated at the Si/SiO_2 interface via the reaction $Si+SiO_2\rightarrow2SiO$ [9,10] is the most likely candidate. In the uncapped sample, oxygen diffusing from the surface reacts with the SiO near the interface and the SiO cannot reach the region where ^{30}Si diffusion is taking place. Therefore, there is no enhancement of Si self-diffusion and only thermal Si self-diffusion is observed. On the other hand, for the capped sample, where the cappings act as perfect barriers against oxygen incorporation, the SiO generated diffuses into the region of implanted ^{30}Si. Therefore, the enhanced self-diffusion via the SiO is observed together with the thermal self-diffusion.

Consequently, we have proposed a model where SiO generated at the Si/SiO_2 interface and diffusing into SiO_2 enhances Si self-diffusion in SiO_2 via the reaction

$$^{30}Si(s)+{}^{28}SiO\Leftrightarrow{}^{28}Si(s)+{}^{30}SiO, \tag{1}$$

$$^{30}Si(s)+{}^{28}Si(s)\Leftrightarrow{}^{28}Si(s)+{}^{30}Si(s). \tag{2}$$

In these equations, Si atoms substituted in the Si sites of SiO_2 [denoted as (s)] diffuse via the kick-out reaction with diffusing SiO. In addition, a simple mechanism of Si self-diffusion, where SiO is not involved, is taken into account for the thermal Si self-diffusion, as described by Eq. (2).

The above model leads to the following set of coupled partial differential equations to describe the diffusion of ^{30}Si in $^{28}SiO_2$:

$$\frac{\partial C_{^{30}Si}}{\partial t}=\frac{\partial}{\partial x}\left(D_{Si}^{SD(th)}\frac{\partial C_{^{30}Si}}{\partial x}\right)-R, \tag{3}$$

$$\frac{\partial C_{^{30}SiO}}{\partial t}=\frac{\partial}{\partial x}\left(D_{SiO}\frac{\partial C_{^{30}SiO}}{\partial x}\right)+R, \tag{4}$$

$$\frac{\partial C_{^{28}SiO}}{\partial t}=\frac{\partial}{\partial x}\left(D_{SiO}\frac{\partial C_{^{28}SiO}}{\partial x}\right)-R, \tag{5}$$

where R is the reaction term for Eq. (1), and described by

$$R=k_f C_{^{30}Si}C_{^{28}SiO}-k_b C_{^{30}SiO}. \tag{6}$$

The Si self-diffusivity is, as a whole, described by

$$D_{Si}^{SD}=D_{Si}^{SD(th)}+D_{SiO}^{SD}\frac{C_{^{28}SiO}(x,t)}{C_{SiO}^{max}}. \tag{7}$$

In these equations, C_x is the concentration of the corresponding species in Eq. (1), $D_{Si}^{SD(th)}$ is the thermal Si self-diffusivity, D_{SiO} is the diffusivity of SiO, and k_f and k_b are the forward and backward rate constants of Eq. (1). In Eq. (3), the thermal Si self-diffusion (Eq. (2)) is represented by the diffusion term with $D_{Si}^{SD(th)}$, and $D_{Si}^{SD(th)}=0.8\exp(-5.2\,eV/kT)\,cm^2/s$ [7] that was experimentally obtained is used for the simulation. In Eq. (7), $D_{SiO}^{SD}=D_{SiO}C_{SiO}^{max}/N_0$ is the Si self-diffusivity via SiO, where N_0 denotes the number of SiO_2 molecules in a unit volume of silicon oxide. Here, C_{SiO}^{max} denotes the maximum SiO concentration in SiO_2 and is described as $C_{SiO}^{max}=3.6\times10^{24}\exp(-1.07\,eV/kT)\,cm^{-3}$ [2]. In Eq. (7), $C_{^{28}SiO}(x,t)$ depends on the depth and annealing times, which will be described below. The ^{28}SiO concentration at the $^{28}Si/^{28}SiO_2$ interface is fixed at C_{SiO}^{max} to describe the generation of SiO at the interface. Reaction (1) is assumed to be so fast that the local equilibrium of the reaction is established, and hence the rate constants are set to be large enough. The parameters deduced from the simulation to fit the experimental profiles of ^{30}Si are D_{SiO}^{SD}, and we consistently obtained $D_{SiO}^{SD}=4\times10^4\exp(-6.2\,eV/kT)\,cm^2/s$ for all samples. Eqs. (3)–(5) were solved numerically by the partial differential equation solver ZOMBIE [11].

Fig. 2 shows the simulated ^{30}Si depth profiles after annealing for 168 h at 1200 °C together with the experimental profiles. For the simulated ^{30}Si profiles, the concentration of $^{30}Si(s)$ is shown because it is about two orders of magnitude larger than that of ^{30}SiO. The simulation results fit the experimental profiles of ^{30}Si for all $^{28}SiO_2$ thicknesses using the same parameter values. This is in contrast to the Si self-diffusivity obtained by a simple fitting, or under the assumption of a constant diffusion coefficient for each profile, which increases with decreasing $^{28}SiO_2$ thickness: 1×10^{-17}, 5×10^{-18}, and $1\times10^{-18}\,cm^2/s$ for 200, 300, and 650 nm, respectively (the contribution from $D_{Si}^{SD(th)}$ at 1200 °C is $1\times10^{-18}\,cm^2/s$ for all thicknesses). In Fig. 2(b), the simulated ^{28}SiO profiles are also shown and the SiO concentration in the region of ^{30}Si increases with decreasing $^{28}SiO_2$ thickness. As expected from Eq. (7), SiO with higher concentration leads to larger enhancement of ^{30}Si diffusion. Therefore, Si self-diffusion becomes faster with decreasing $^{28}SiO_2$ thickness. This thickness dependence arises because the SiO diffusion is so slow that the SiO concentration critically depends on the distance from the Si/SiO_2 interface, where the SiO is generated. In addition, the profile of SiO for the 650-nm-thick sample

shows that the SiO concentration is so small that Si self-diffusion cannot be explained only by the kick-out diffusion via SiO (Eq. (1)). This is the evidence for the existence of the two mechanisms (with and without SiO), as described above.

From the simulation, we found that the SiO concentration in the near-surface region becomes higher at longer annealing times until it reaches the maximum concentration. Fig. 3 shows the simulated ^{30}Si and SiO profiles in the 300-nm-thick sample after annealing for 6 and 30 h at 1250 °C. The Si self-diffusivities, assuming a constant diffusion coefficient, show an enhancement of factor of 4.5 and are 1×10^{-17} cm^2/s for 6 h and 4.5×10^{-17} cm^2/s for 30 h. This time dependence arises because the SiO diffusion is so slow that more SiO molecules are arriving from the interface with time, and the self-diffusivity, assuming a constant diffusion coefficient, therefore increases for a longer annealing time. In order to confirm this prediction, we performed an experiment for the time dependence. The experimental results are shown in Fig. 3, and the simulated and experimental profiles almost coincide and this confirms the validity of our model.

For the experiments of B diffusion in SiO_2, the $^{28}SiO_2$ samples were also implanted with ^{11}B at 25 keV to a dose of 5×10^{13} cm^{-2}. Fig. 4 shows the experimental B profiles after annealing at 1200 °C for 24 h. In the same way as Si self-diffusion, the B diffusion demonstrates a clear dependence on the thickness of the $^{28}SiO_2$ layer; the shorter the distance from the Si/SiO_2 interface, the higher the B diffusivity in SiO_2. In a similar manner to Si self-diffusion, the B diffusion profiles were simulated assuming the enhanced B diffusion reaction via SiO,

$$B(s) + {}^{28}SiO \Leftrightarrow {}^{28}Si(s) + BO. \quad (8)$$

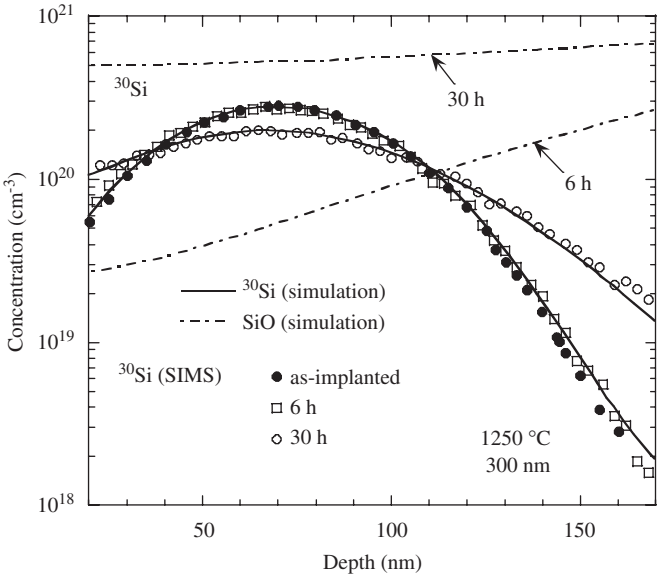

Fig. 3. Simulated and experimental ^{30}Si depth profiles, and simulated SiO profiles in the 300-nm-thick sample. Samples were annealed at 1250 °C for 6 and 30 h.

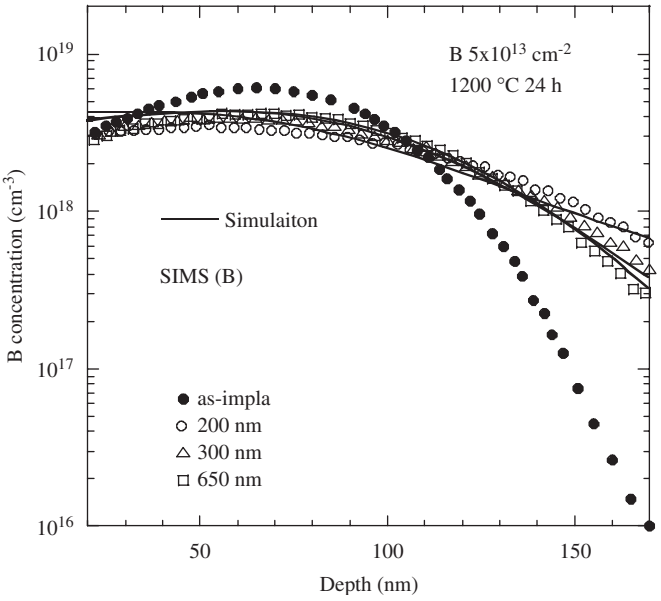

Fig. 4. Simulated and experimental B depth profiles in SiO_2 samples with various thicknesses. Samples were implanted with B to a dose of 5×10^{13} cm^{-2} and annealed at 1200 °C for 24 h.

As shown in Fig. 4, the simulation results also fit the experimental B profiles for all the thicknesses using the same parameter values. These results show that SiO generated at the Si/SiO_2 interface enhances not only Si self-diffusion but also B diffusion in SiO_2. We mention that the time-dependent diffusivity was also observed for B diffusion [12].

The present results imply that the Si/SiO_2 interface could influence silicon processes involving B and Si diffusion. The $D_{SiO} = 3.4\times10^2\exp(-5.2\,\mathrm{eV}/kT)\,\mathrm{cm}^2/\mathrm{s}$ deduced has the value of $\sim4\times10^{-17}$ cm^2/s at 1100 °C, and the diffusion length for 10 s annealing is $2(D_{SiO}t)^{1/2}\sim0.4$ nm. This estimation indicates that SiO from the interface may affect the phenomena in the bulk in nitride-capped samples, or during non-oxidizing silicon processes, when the material thickness is down to 1 nm. In addition, the SiO generated at the interface enhances B diffusion by one order of magnitude, and therefore, the effect of the Si/SiO_2 interface becomes more serious with decreasing the SiO_2 thickness.

3. Si self-diffusion in Si at low temperatures

The understanding of the Si self-diffusion mechanism is indispensable for the development of nano-scale silicon diffusion simulators because the self-diffusion plays a key role in the impurity diffusion and recovering of the implantation damage. In Si nano-processing, annealing temperatures become lower in order to reduce the impurity diffusion during the process, and therefore, accurate values of the Si self-diffusivity at low temperatures are highly desired. In general, the Si self-diffusivity in Si is given by

$$D_{Si}^{SD} = D_I^{SD} + D_V^{SD}, \quad (9)$$

where the two terms represent the contributions of self-interstitials (I) and vacancies (V). Using isotopically enriched Si substrates, Si self-diffusivity was directly measured at a temperature range between 855 and 1388 °C and the diffusivity showed a single diffusion enthalpy, which indicates that self-interstitials dominate Si self-diffusion at this temperature range [13]. In this experiment, SIMS measurements were used to observe the Si diffusion profiles. However, accurate determination of the self-diffusivity at low temperatures $T<850\,^{\circ}\mathrm{C}$ from SIMS profiles is difficult because the diffusion length after reasonable annealing duration is still too small for the depth resolution of SIMS. This difficulty was overcome by detection of the very small diffusion length in isotope superlattices of Si using Raman spectroscopy [4].

A $^{28}Si_n/^{30}Si_n$ isotope superlattice with $n=20$ atomic layers was grown by solid-source molecular beam epitaxy [4,14,15]. The degree of intermixing at the $^{28}Si/^{30}Si$ interfaces is less than a couple of monolayers in the as-grown sample [15]. The intrinsic carrier concentration of the sample was $1\times10^{18}\,\mathrm{cm}^{-3}$ at the lowest diffusion annealing temperature of 735 °C, which ensured that the sample remained intrinsic and the Fermi level effect did not play a role. The Raman measurements of the longitudinal optical (LO) phonon frequencies were performed using an Ar^+ 514.5 nm line. The spectral resolution was $0.7\,\mathrm{cm}^{-1}$ and the measurements were done at 8 K. Fig. 5 shows Raman spectra of the $^{28}Si_{20}/^{30}Si_{20}$ isotope superlattice annealed at 795 °C for various annealing times. In the as-grown sample, three small peaks due to the artificial mass periodicity of Si isotopes are clearly observed on the left side of the large LO peak of ^{nat}Si. These peaks correspond to $LO_3(^{28}Si)$, $LO_5(^{28}Si)$, and $LO_1(^{30}Si)$ in the order from the higher to lower Raman shifts, respectively, which are the same as for Ge isotope superlattices [16]. Here the notations $LO_m(^{28}Si)$ and $LO_m(^{30}Si)$ represent the mth confined vibrational mode in the ^{28}Si and ^{30}Si layers, respectively. The peak positions of the confined phonons shift systematically with the diffusion annealing time because interdiffusion of isotopes at every $^{28}Si/^{30}Si$ interface in the superlattices occurs exactly in the same manner. For example, as annealing time increases, the lowest Raman shift peak $LO_1(^{30}Si)$ disappears, while the $LO_1(^{28}Si)$ hidden in the ^{nat}Si substrate peak emerges after 24 h annealing. The Si self-diffusivity for a given temperature is determined from tracing of these peak positions as a function of annealing times [4].

The temperature dependence of the Si self-diffusivity determined by the present method (filled circles) is shown in Fig. 6 together with those determined previously from SIMS measurements of isotope heterostructures (open squares) [13] and from the study of Zn in-diffusion in Si (open triangles) [17]. The Si self-diffusivities determined by the present method agree very well with those reported in Refs. [13,17] in the overlapping temperature range between 850 and 900 °C. Based on the contribution of self-interstitials to Si self-diffusion from Ref. [13], we obtained the Si self-diffusivity D_{Si}^{SD} for $T=735$–1388 °C in Eq. (9) as

$$D_I^{SD}=2.18\times10^{3}\exp\left(\frac{-4.95\,\mathrm{eV}}{kT}\right)(\mathrm{cm}^2/\mathrm{s}),$$
$$D_V^{SD}=2.3\times10^{-3}\exp\left(\frac{-(3.6^{+0.3}_{-0.1})\,\mathrm{eV}}{kT}\right)(\mathrm{cm}^2/\mathrm{s}). \quad (10)$$

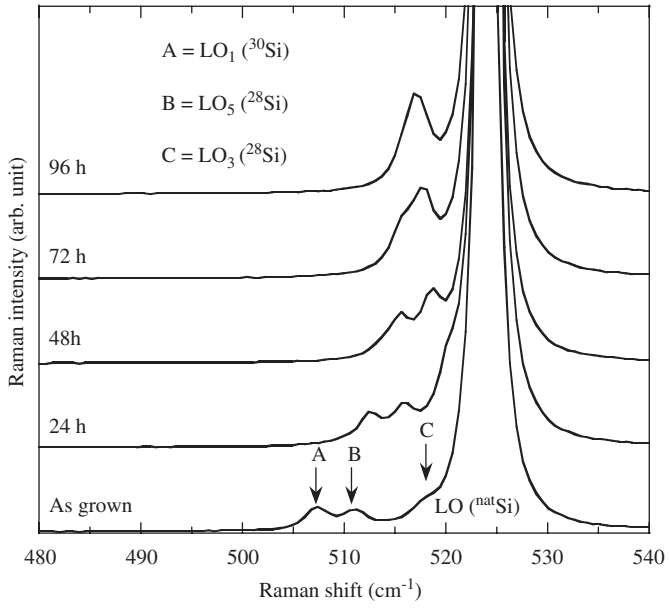

Fig. 5. Raman spectra of the $^{28}Si_{20}/^{30}Si_{20}$ isotope superlattice annealed at 795 °C for various annealing times.

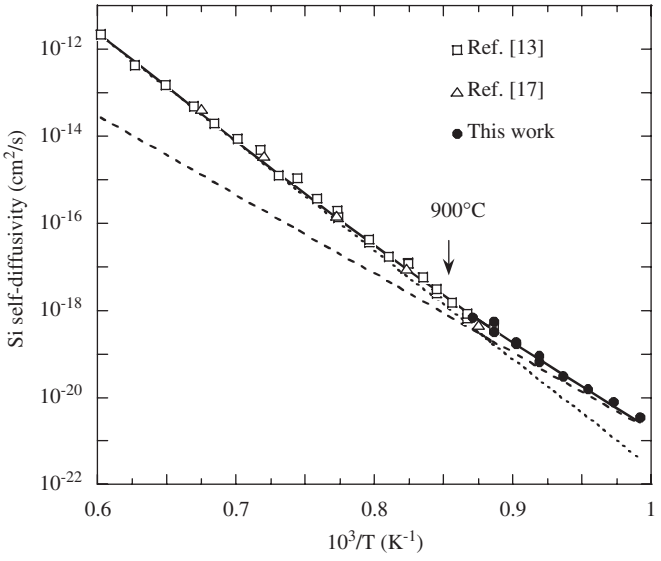

Fig. 6. Temperature dependence of the Si self-diffusivity. Results in the present method are shown by filled circles together with those determined previously from SIMS measurements of isotope heterostructures (open squares) [13] and from the study of Zn in-diffusion in Si (open triangles) [17]. The solid line represents the total self-diffusivity D_{Si}^{SD} in Eq. (9). Broken and dotted lines show the contributions of self-interstitials [13] and vacancies, respectively.

The vacancy activation enthalpy is given by the sum of the vacancy formation and migration enthalpies. Recent *ab initio* calculations yield the vacancy formation enthalpy confined between 3.1 and 3.6 eV [18–20], and these values lead to the vacancy migration enthalpy <0.8 eV, with the most probable value around 0.4 eV. This value agrees with 0.45 eV obtained by an electron paramagnetic resonance study [21].

In Fig. 6, we found the change in the activation enthalpy at around 900 °C, indicating that the Si self-diffusion mechanism changes from self-interstitials in the higher temperature range to vacancies in the lower temperature range. The present result shows that the Si self-diffusivity at $T<900$ °C is much larger than that estimated by extrapolating the values of D_I^{SD} to the lower temperature range. It is well-known that arsenic (As) diffusion in Si has appreciable components via both the interstitial and vacancy mechanisms [22]. In addition, Si self-diffusion plays a key role in the formation of implantation-induced defects, which mainly occurs during the early stages of annealing, that is, in a lower temperature range. This means that the nano-scale diffusion simulation requires precise values of Si self-diffusivity, especially at lower temperatures, and therefore, our finding for the crossover at 900 °C is of great technological importance.

4. Simultaneous observation of self- and impurity-atom behavior in Si

Shallow junction formation is one of the most important issues in CMOS processing, and with the scaling down of CMOS devices shallower impurity profiles with higher concentration are required. The quantitative understanding of behaviors and reactions of defects and impurity is crucial to precisely control the distribution, concentration, and activation of the impurities in Si. For n-type impurities, As is widely used because it is suitable for the formation of shallow impurity profiles with higher concentration. Diffusion of high-dose implanted As in Si during post-implantation annealing is a complex phenomena. Concerning diffusion mechanism, both the interstitial and vacancy mechanisms are involved, as described above. In addition, {3 1 1} self-interstitial clusters produced by ion-implantation damage induce transient enhanced diffusion (TED), and Ostwald ripening of the clusters play an important role for TED [23,24]. Furthermore, end-of-range (EOR) defects form at the amorphous/crystalline (a/c) interface [25] acting as both a sink for and source of self-interstitials [26], and Ostwald ripening of the defects reduces their efficiency as a source of self-interstitials [27,28]. Therefore, not only As diffusion but also the behavior of Si atoms should be precisely investigated for the simulation of the time evolution of these implantation-induced defects. Here we report the simultaneous observation of the behavior of As impurities and Si atoms in Si isotope superlattices using SIMS and transmission electron microscopy (TEM). This enables precise determination of (1) the degree of mixing of Si host atoms induced by implantation and (2) the diffusion of Si point defects during post-implantation annealing.

$^{75}As^+$ ions are implanted at 25 or 60 keV with doses of 1×10^{13} to 1×10^{15} cm^{-2} into ^{28}Si (2.7 nm)/^{30}Si (2.7 nm) isotope superlattices. Fig. 7(a) shows the SIMS profiles of ^{28}Si, ^{30}Si, and ^{75}As in the as-implanted samples with the dose of 3×10^{14} cm^{-2}. This high-dose implantation induces mixing of ^{28}Si and ^{30}Si into the depth of 70 nm, while the dose of 1×10^{13} cm^{-2} leads to no observable changes in the depth profiles. Although the As concentration profile has a peak at around 40 nm, the amount of Si mixing shows its maximum at the 20–30 nm region. We have developed a model based on convolution integral to simulate the SIMS profile of mixed ^{28}Si and ^{30}Si [29]. Using this model, we obtained the length of Si displacements, or mixing length, as a function of the depth. The mixing length deduced from the profiles of ^{28}Si and ^{30}Si is shown in Fig. 7(b). As expected from the amount of Si mixing, the mixing length has its maximum at around 25 nm in depth. In addition, we observed the cross-sectional TEM images of the as-implanted samples and measured the thickness of the surface amorphous layer created by implantation. The TEM result of the 3×10^{14} cm^{-2} dose sample in Fig. 7(b) shows that the Si amorphous layer extends up to the depth of about 70 nm, where an abrupt a/c interface is formed. A comparison of the TEM result with the mixing length deduced above, we found that the Si amorphization occurs when the mixing length is larger than 0.5 nm. These observations allow us to estimate how the Si atoms are displaced and then the damages are generated during

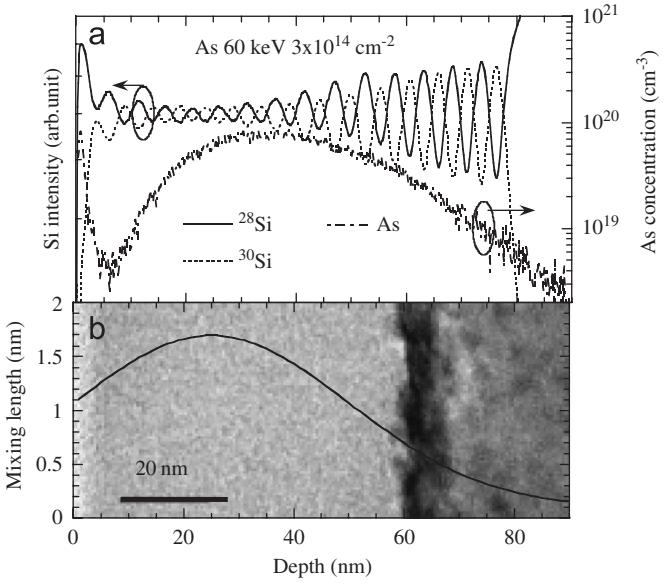

Fig. 7. (a) Depth profiles of ^{28}Si, ^{30}Si, and ^{75}As in the as-implanted ^{28}Si/^{30}Si sample with 60 keV, 3×10^{14} cm^{-2} As implantation. (b) Si mixing length deduced from the ^{28}Si/^{30}Si profiles and cross-sectional TEM image of the sample.

implantation, which is indispensable to precisely predict the implantation-induced defect distributions.

In order to observe the diffusion of Si point defects during post-implantation annealing, the ^{nat}Si (10 nm)/^{28}Si (10 nm) isotope superlattice samples implanted with As at 60 keV to a dose of 3×10^{14} cm^{-2} were annealed. Fig. 8 shows the SIMS profiles of ^{30}Si and ^{75}As before and after annealing at 850 °C for 16 h. After the annealing, the ^{30}Si profile is broadened, especially in the region between 30 and 60 nm in depth, where the annealing broadens the profile larger than what is estimated from the Si self-diffusivity at 850 °C obtained in Section 3. This depth region 30–60 nm almost coincides with the depth where the As concentration is the highest. Thus, the enhanced diffusion of ^{30}Si arises predominantly by the Fermi level effect after this long annealing time. In this experiment, EOR defects are formed at the a/c interface (70 nm in depth); however, their efficiency as a source of self-interstitials is reduced due to Ostwald ripening after a long time annealing. Therefore, Si self-interstitials are almost in equilibrium and hence Fermi level effect plays an important role in the diffusion. On the other hand, the ^{30}Si profile was significantly broadened in the region deeper than the a/c interface after short or medium time annealing (<4 h). In this time region, EOR defects are still active as a source of self-interstitials. These Si self-interstitials enhance the Si diffusion in the region deeper than the a/c interface, where impurity concentration is low and Fermi level effect is not significant. Therefore, from these simultaneous observations of impurity and Si atoms, we can quantitatively determine the depth distribution of Si self-interstitials, which is essential for developing nano-scale diffusion simulators.

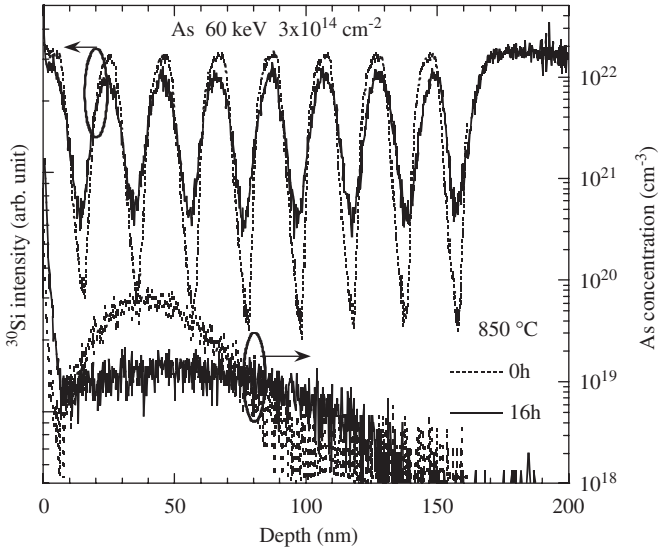

Fig. 8. Depth profiles of ^{30}Si and ^{75}As in the ^{nat}Si/^{28}Si isotope superlattice. Oscillating dashed- and solid-lines represents concentrations of ^{30}Si before and after annealing, respectively, at 850 °C for 16 h. The bottom dashed- and solid-lines represent concentrations of ^{75}As before and after the annealing, respectively.

5. Summary

Nano-scale Si processing requires the basic understanding of the transient and non-equilibrium behaviors of defect interactions. Experiments using isotopically controlled silicon heterostructures are very effective to indentify what types of kinetics and reactions are relevant to the nano-processing. We showed that Si species, most likely SiO, generated at the Si/SiO_2 interface and diffusing into SiO_2 enhance Si self-diffusion in SiO_2. The quantitative models and the diffusion simulation based on the experimental results were presented. The simulation results indicate that SiO from the interface may affect the phenomena in the bulk even in capped samples when the material thickness is down to 1 nm. Next, precise measurements of the Si self-diffusivity in Si using Si isotope experiments were described. The Si self-diffusivity showed the crossover from the self-interstitial mechanism at the high temperatures to the vacancy mechanism at the low temperatures. The result shows that the Si self-diffusivity in Si at low temperatures is much larger than that estimated by extrapolating the value at high temperatures. This finding is of great technological importance because the nano-scale diffusion simulation requires precise values of the Si self-diffusivity, especially at lower temperatures. Furthermore, the simultaneous observation of the behavior of As impurities and Si atoms in Si isotope superlattices was presented. The investigations of the as-implanted samples allow us to estimate how the Si atoms are displaced and then the damages are generated during implantation. In addition, simultaneous diffusion of As and Si atoms during post-implantation annealing was observed, which enables a quantitative determination on the depth distribution of Si self-interstitials.

Acknowledgments

The present research was a collaboration with H. Kageshima and K. Shiraishi and with Selete (Semiconductor Leading Edge Technologies, Inc.). We thank A. Takano for SIMS measurements and H. Oshikawa for TEM measurements. The work has been supported in part by the Research Program on Collaborative Development of Innovative Seeds by JST (Japan Science and Technology Agency) and in part by the Special Coordination Funds for Promoting Science and Technology for INQIE.

References

[1] S. Fukatsu, T. Takahashi, K.M. Itoh, M. Uematsu, A. Fujiwara, H. Kageshima, Y. Takahashi, K. Shiraishi, U. Gösele, Appl. Phys. Lett. 83 (2003) 3897.
[2] M. Uematsu, H. Kageshima, Y. Takahashi, S. Fukatsu, K.M. Itoh, K. Shiraishi, U. Gösele, Appl. Phys. Lett. 84 (2004) 876.
[3] M. Uematsu, H. Kageshima, Y. Takahashi, S. Fukatsu, K.M. Itoh, K. Shiraishi, Appl. Phys. Lett. 85 (2004) 221.
[4] Y. Shimizu, M. Uematsu, K.M. Itoh, Phys. Rev. Lett. 98 (2007) 095901.

[5] J.R. Pfiester, L.C. Parrollo, F.K. Baker, IEEE Electron. Device Lett. 11 (1990) 247.
[6] G.D. Wilk, R.M. Wallace, J.M. Anthony, J. Appl. Phys. 89 (2001) 5243.
[7] T. Takahashi, S. Fukatsu, K.M. Itoh, M. Uematsu, A. Fujiwara, H. Kageshima, Y. Takahashi, K. Shiraishi, J. Appl. Phys. 93 (2003) 3674.
[8] S. Fukatsu, K.M. Itoh, M. Uematsu, H. Kageshima, Y. Takahashi, K. Shiraishi, Jpn. J. Appl. Phys. 43 (2004) 7837.
[9] T.Y. Tan, U. Gösele, Appl. Phys. Lett. 40 (1982) 616.
[10] G.K. Celler, L.E. Trimble, Appl. Phys. Lett. 54 (1989) 1427.
[11] W. Jüngling, P. Pichler, S. Selberherr, E. Guerrero, H.W. Pötzl, IEEE Trans. Electron. Devices 32 (1985) 156.
[12] M. Uematsu, H. Kageshima, Y. Takahashi, S. Fukatsu, K.M. Itoh, K. Shiraishi, J. Appl. Phys. 96 (2004) 5513.
[13] H. Bracht, E.E. Haller, R. Clark-Phelps, Phys. Rev. Lett. 81 (1998) 393.
[14] T. Kojima, R. Nebashi, K.M. Itoh, Y. Shiraki, Appl. Phys. Lett. 83 (2003) 2318.
[15] Y. Shimizu, K.M. Itoh, Thin Solid Films 508 (2006) 160.
[16] J. Spitzer, T. Ruf, M. Cardona, W. Dondl, R. Schorer, G. Abstreiter, E.E. Haller, Phys. Rev. Lett. 72 (1994) 1565.
[17] H. Bracht, N.A. Stolwijk, H. Mehrer, Phys. Rev. B 52 (1995) 16542.
[18] M.I.J. Probert, M.C. Payne, Phys. Rev. B 67 (2003) 075204.
[19] J. Lento, R.M. Nieminen, J. Phys.: Condens. Matter 15 (2003) 4387.
[20] F. El-Mellouhi, N. Mousseau, P. Ordejón, Phys. Rev. B 70 (2004) 205202.
[21] G.D. Watkins, Mater. Res. Soc. Symp. Proc. 469 (1997) 139.
[22] T.Y. Tan, U. Gösele, Appl. Phys. A 37 (1985) 1.
[23] P.A. Stolk, H.-J. Gossmann, D.J. Eaglesham, D.C. Jacobson, C.S. Rafferty, G.H. Gilmer, M. Jaraíz, J.M. Poate, H.S. Luftman, T.E. Haynes, J. Appl. Phys. 81 (1997) 6031.
[24] M. Uematsu, Jpn. J. Appl. Phys. 36 (1997) L982.
[25] K.S. Jones, S. Prussin, E.R. Weber, Appl. Phys. A 45 (1988) 1.
[26] M. Uematsu, Jpn. J. Appl. Phys. 37 (1998) 5866.
[27] C. Bonafos, D. Mathiot, A. Claverie, J. Appl. Phys. 83 (1998) 3008.
[28] M. Uematsu, Jpn. J. Appl. Phys. 38 (1999) L1213.
[29] Y. Shimizu, A. Takano, M. Uematsu, K.M. Itoh, Appl. Phys. Lett., submitted for publication.